JOURNAL OF VIROLOGY, May 2005, p. 5743–5751 Vol. 79, No. 9
0022-538X/05/$08.00+0 doi:10.1128/JVI.79.9.5743–5751.2005

Evaluation of the Conformational Switch Model for Alfalfa Mosaic Virus RNA Replication

Jessica E. Petrillo, Gail Rocheleau, Brenna Kelley-Clarke, and Lee Gehrke*

Harvard-MIT Division of Health Sciences and Technology and Department of Microbiology and Molecular Genetics, Harvard Medical School, Boston, Massachusetts

Received 13 September 2004/Accepted 23 December 2004

Key elements of the conformational switch model describing regulation of alfalfa mosaic virus (AMV) replication (R. C. Olsthoorn, S. Mertens, F. T. Brederode, and J. F. Bol, EMBO J. 18:4856–4864, 1999) have been tested using biochemical assays and functional studies in nontransgenic protoplasts. Although comparative sequence analysis suggests that the 3′ untranslated regions of AMV and ilarvirus RNAs have the potential to fold into pseudoknots, we were unable to confirm that a proposed pseudoknot forms or has a functional role in regulating coat protein-RNA binding or viral RNA replication. Published work has suggested that the pseudoknot is part of a tRNA-like structure (TLS); however, we argue that the canonical sequence and functional features that define the TLS are absent. We suggest here that the absence of the TLS correlates directly with the distinctive requirement for coat protein to activate replication in these viruses. Experimental data are evidence that elevated magnesium concentrations proposed to stabilize the pseudoknot structure do not block coat protein binding. Additionally, covarying nucleotide changes proposed to reestablish pseudoknot pairings do not rescue replication. Furthermore, as described in the accompanying paper (L. M. Guogas, S. M. Laforest, and L. Gehrke, J. Virol. 79:5752–5761, 2005), coat protein is not, by definition, inhibitory to minus-strand RNA synthesis. Rather, the activation of viral RNA replication by coat protein is shown to be concentration dependent. We describe the 3′ organization model as an alternate model of AMV replication that offers an improved fit to the available data.

Regulation of the switch between translation and replication is a fundamental problem in understanding the biology of positive-stranded RNA viruses. Olsthoorn et al. (22) published the conformational switch model to propose a mechanism for regulating the switch in alfalfa mosaic virus (AMV). The conformational switch model asserts that the 3′ termini of the viral RNAs fold into two mutually exclusive conformations that have distinct functions, that is, pseudoknotted (coat protein [CP]-free) and extended (CP-bound) forms. In the absence of viral CP, the RNA 3′ terminus is said to adopt a pseudoknotted tRNA-like structure (TLS) that would make it structurally homologous to many other bromovirus RNAs. Regions 1 and 2 of the viral RNA (see Fig. 1B) have the potential to form a pseudoknot, and nucleotide variations across the ilarviruses suggest covarying substitutions that would maintain the long-range pseudoknot pairing (22). Equally interesting, however, is the fact that the nucleotides in region 3 of the viral RNAs also covary with changes in region 2, thereby also maintaining the potential to form the downstream hairpin by short-range folding (hairpin from nucleotides 869 through 877) (Fig. 1B). Recent data confirm that hairpin from nucleotides 869 through 877 is present in the crystal structure of the 39-nucleotide 3′-terminal RNA fragment in complex with the RNA binding domain of the viral CP (11).

The conformational switch model proposes that CP binding to the 3′ termini disrupts the pseudoknot formed by the interaction of regions 1 and 2 (Fig. 1B), inducing an extended conformation that is no longer competent for recognition by the viral-RNA-dependent RNA polymerase. In this way, CP binding is proposed to inhibit minus-strand synthesis, inducing the switch to asymmetric plus-sense RNA synthesis. Because CP binding has also been linked to viral RNA translation (20, 21), Olsthoorn et al. propose that its role in replication is to enhance the translation of the replicase proteins and to regulate the switch to plus-strand synthesis. To accomplish this, the conformational switch model requires that the viral RNAs are free of CP during minus-strand synthesis but bound to CP during translation and plus-strand synthesis. To date, there is no evidence that CP cycles on and off the 3′ terminus of the viral RNAs during the viral life cycle.

Here, we present a detailed evaluation of the conformational switch model and report experimental evidence that is consistent with an alternate model, referred to herein as the 3′ organization model. In contrast to the conformational switch model, we provide data demonstrating that CP peptide binding compacts, rather than extends, the 3′ RNA termini. Moreover, elevated magnesium levels are not associated with specific inhibition of CP binding to the wild-type 3′ untranslated region (UTR). Additionally, functional analyses reveal that in electroporated nontransgenic protoplasts, compensatory mutations introduced into variant RNA3 constructs to restore pseudoknot base pairing do not rescue replication. We propose that the differences in functional data from the two laboratories may be traced to the use of wild-type cells (described here) versus in vitro analysis and the use of transgenic cells that overexpress replicase proteins (22). The accumulated evidence presented here, along with functional data presented in the accompanying paper (12) and the crystal structure of the AMV RNA-peptide complex (11), suggest that CP binding organizes

* Corresponding author. Mailing address: HST Division, MIT E25-545, 77 Massachusetts Avenue, Cambridge, MA 02139. Phone: (617) 253-7608. Fax: (509) 357-7835. E-mail: lee_gehrke@hms.harvard.edu.

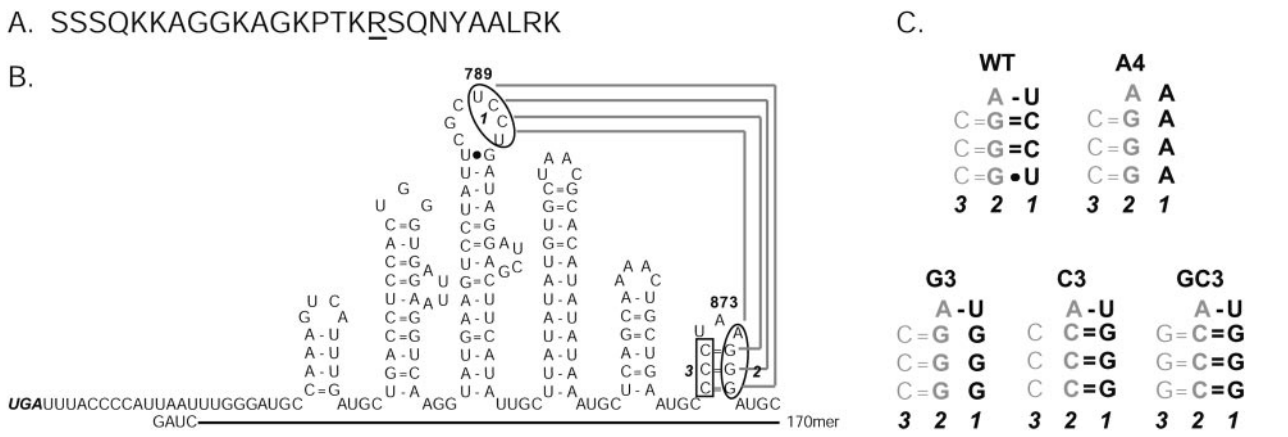

FIG. 1. (A) Amino acid sequence of peptide CP26, representing the N-terminal 26 amino acids and the RNA binding domain of the viral CP. The arginine at position 17, essential for RNA binding (2), is underlined. (B) Sequence and secondary structure of the 3′ untranslated region of genomic AMV RNA3 and subgenomic RNA4. The secondary structure is based on computer folding methods and enzymatic structure mapping data (23). The underlining shows the boundaries of the ~170-nucleotide 3′ UTR fragments used in the experiments. The gray lines indicate the putative pseudoknot structure reported by Olsthoorn et al. (22). Region 1 nucleotides are proposed to pair with region 2 nucleotides to form a pseudoknot structure (22). (C) Pseudoknot mutations used in this study. Regions are indicated beneath each group by italic numbers. Nucleotides that form the proposed pseudoknot interactions (regions 1 and 2) are printed in bold. Nucleotides that interact to form the 3′-terminal hairpin (regions 2 and 3) are printed in gray. WT, wild type.

the 3′ termini of the viral RNAs for activation of early viral RNA replication.

MATERIALS AND METHODS

In vitro RNA transcription. Small RNAs (<200 nucleotides in length) were transcribed in vitro using the Megashortscript T7 kit (Ambion, Austin, Tex.) according to the manufacturer's instructions. RNA transcripts corresponding to the 3′-terminal 170 nucleotides of AMV RNA4 (AMV nucleotides 718 through 881) were transcribed from linearized plasmid DNA. Probe RNAs used in electrophoretic mobility shift assays (EMSA) were radiolabeled during transcription by including 20 μCi of [α-^{32}P]UTP in the presence of 5.6 mM ATP, CTP, GTP, and 0.56 mM UTP. The RNAs were purified by electrophoresis into 5% denaturing polyacrylamide gels, visualized by UV light shadowing, and eluted overnight at 4°C in elution buffer (5).

Capped infectious viral RNA transcripts for in vivo replication studies were generated from linearized plasmid DNAs by using the Ambion mMessage Machine kit. Following the incubation period, the RNAs were precipitated by the addition of lithium chloride according to the manufacturer's protocol. Constructs encoding infectious clones of AMV RNAs were prepared as described previously (16, 26). The RNA4 clone was provided by L. Sue Loesch-Fries (18). To provide unequivocal evidence of RNA replication by detection of subgenomic RNA4, replication was activated in some experiments by a truncated RNA4 construct (AMV4-trUTR) wherein nucleotides 719 through 842 of the 3′ untranslated region (Fig. 1B) were deleted (26).

Site-directed mutagenesis of RNAs. Pseudoknot mutants A4, G3, GC3, and C3 (22) were introduced into infectious RNA3 and RNA4 constructs to assay the effects of these mutations on replication and translation, respectively. Additionally, these mutations were introduced into a 3′ UTR transcription construct consisting of the 3′-terminal 170 nucleotides of AMV RNA4 (AMV nucleotides 718 through 881). The nucleotide mutagenesis was carried out with the QuikChange kit (Stratagene) according to the manufacturer's recommendations. The nucleotide changes were confirmed by sequence analysis.

Size exclusion chromatography. Viral RNA and RNA-peptide complexes were analyzed by chromatography on a Sephacryl 200 column by using an AKTA high-pressure liquid chromatography (HPLC) instrument (Amersham Biosciences) (4, 32). Approximately 5 μg of RNA was injected onto the column in the absence or presence of excess peptide. RNA-peptide complexes were formed as described previously (1). Briefly, the 170-nucleotide 3′ UTR RNA was renatured by heating to 65°C for 3 min in 10 mM Tris-HCl–50 mM NaCl–3 mM $MgCl_2$–0.1 mM EDTA. Free 170-mer 3′ UTR RNA or RNA bound to the CP26 peptide was injected onto a Sephacryl 200 column in 10 mM Tris-HCl–50 mM NaCl–0.1 mM EDTA. The chromatography buffer was 50 mM NaCl–0.1 mM EDTA–10 mM Tris-HCl, pH 7.5. The column was run at 0.7 ml/min on an Amersham Biosciences System AKTA HPLC unit. The absorbance at 254 nm was monitored continuously.

EMSA. The rigor and utility of the electrophoretic mobility bandshift assay as a sensitive indicator of the size and shape of nucleoprotein complexes has been well documented (10, 19, 30). Band shift assays were carried out as described previously (3, 14). Briefly, RNA was renatured by heating in REN buffer (3 mM magnesium chloride, 50 mM NaCl, 10 mM Tris-HCl buffer [pH 7.5]) at 65°C for 3 min, followed by slow cooling to room temperature for 15 min. Ten-microliter binding reactions contained 20 nM RNA and included varying amounts of AMV CP or AMV CP26 peptide in binding buffer (10 mM Tris-HCl [pH 7.5], 50 mM NaCl, 0.1 mM EDTA, 5% glycerol, 0.15 mg of yeast tRNA/ml). Additional magnesium was included in the REN buffer and binding buffer as indicated in the figure legends. AMV CP was purified from virions (15). Peptides were HPLC purified, and the concentrations were determined by amino acid analysis. Formation of RNA-protein complexes was analyzed by electrophoresis into a 10% native polyacrylamide gel (acrylamide/bis ratio of 46:1) with 0.5× TBE (45 mM Tris-borate, 1 mM EDTA) as electrophoresis buffer. RNA and RNA-protein complexes were visualized by autoradiography. The approximate K_d of the CP-RNA interaction was determined visually as the protein or peptide concentration at which 50% of the RNA was bound by protein or peptide (6).

Viral RNA transfection and RNA replication assays. In vitro-transcribed, capped AMV RNAs were transfected by electroporation into tobacco protoplasts prepared from *Nicotiana tabacum* NT-1 cells grown in liquid culture (31). Cells were inoculated in maintenance medium (1× Murashige and Skoog salt mixture, 88 mM sucrose, 0.6 mM *myo*-inositol, 1 mg of thiamine-HCl/liter, 0.2 mg of 2,4-dichloro-phenoxyacetic acid/liter, pH 5.8), incubated at 28°C with shaking for 3 days, harvested by gentle sedimentation, and washed twice in 0.4 M mannitol–20 mM morpholineethanesulfonic acid (MES), pH 5.8. The cells were resuspended in 0.4 M mannitol–20 mM MES [pH 5.8]–1% cellulase (Calbiochem)–0.1% pectolyase (Sigma), transferred to petri dishes, and incubated for 1 h in the dark with gentle shaking (60 rpm) to digest the cell walls. After sedimenting of the cells by centrifugation at 100 × *g* for 2 min, they were washed twice by resuspension in 0.4 M mannitol–20 mM MES (pH 5.8) and counted. After a final sedimentation step, the protoplasts were resuspended at a concentration of 5 × 10^6 cells/ml in 0.4 M mannitol–20 mM MES (pH 5.8). For the replication assay, 200 μl of the protoplast suspension (10^6 cells) was mixed with 600 μl of ice-cold electroporation buffer (0.14 M NaCl, 3 mM KCl, 1.5 mM KH_2PO_4, 8 mM Na_2HPO_4, 0.4 M D-mannitol, pH 6.5) containing 12 μg of a mixture of in vitro-transcribed AMV RNAs at molar ratios of 1:1:1:2 (4.4 μg of RNA1, 3.1 μg of RNA2, 2.4 μg of RNA3, 2.1 μg of RNA4). The protoplasts were electroporated at 300 V and 325 μF and then allowed to recover on ice for 20 min. The cells were diluted into 5 ml of protoplast medium (1× Murashige and

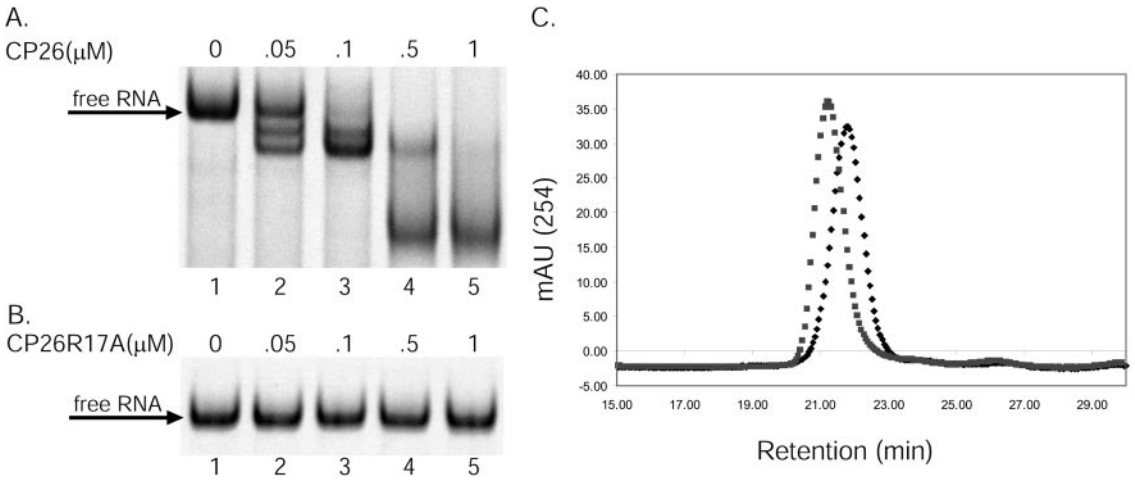

FIG. 2. Peptide binding compacts the 3′ UTR RNA conformation. (A) Electrophoretic mobility shift analysis of peptide CP26 binding to the 3′-terminal, 170-nucleotide, 3′ untranslated region of AMV RNA4. The RNA concentration in the binding reactions was 20 nM. The concentrations of peptide present in the binding reactions are shown above the gel lanes. (B) Control binding experiments showing that the CP26R17A peptide does not bind the viral RNA. (C) Gel filtration analysis of free and peptide-bound AMV RNA. Black diamonds, RNA plus peptide CP26; gray squares, RNA only. Further details are found in Materials and Methods.

Skoog salt mixture, 88 mM sucrose, 0.6 mM *myo*-inositol, 1 mg of thiamine-HCl/liter, 0.2 mg of 2,4-dichloro-phenoxyacetic acid/liter, 0.4 M mannitol, pH 5.8) and incubated at 28°C for 48 h.

AMV RNA analysis. Total protoplast RNA was isolated using Trizol (Gibco BRL) according to the manufacturer's instructions. Protoplasts from 3 ml of the suspension were sedimented and resuspended in 1 ml of Trizol reagent. Precipitated RNA was sedimented by centrifugation, and the resulting pellet was washed with 70% ethanol and resuspended in water at 2 μg/μl. A 1% (wt/vol) agarose gel was used to separate the RNAs for Northern blot hybridization analysis. After dissolving of the agarose in water with heating, the solution was allowed to cool to about 65°C, at which time 0.1 volume of 10× morpholinepropanesulfonic acid solution (0.2 M MOPS [Sigma], 50 mM NaOAc, 5 mM EDTA, pH 7, adjusted with NaOH) and 0.01 volume of stock (37.5%) formaldehyde were added in a fume hood. The RNAs were denatured in a total volume of 20 μl by using a 3:1 ratio of denaturation buffer to RNA. The stock denaturation buffer was prepared by mixing 100 μl of deionized formamide, 25 μl of 10× MOPS solution, 25 μl of formaldehyde, 5 μl of a 2.5% solution of bromophenol blue and xylene cyanol dyes, and 0.1 μl of a 1-mg/ml solution of ethidium bromide. The RNAs were denatured by heating to 65°C for 15 min, quick-cooled, and immediately loaded onto the gel. After electrophoresis, the RNAs were transferred to nitrocellulose membranes (TurboBlotter; Schleicher and Schuell) and cross-linked to the membrane with UV light (GS Gene Linker; Bio-Rad). Prehybridization solution was prepared by combining 6 ml of phosphate-EDTA buffer (0.2 M NaH_2PO_4, 0.6 M Na_2HPO_4, 5 mM EDTA), 3 ml of 20% sodium dodecyl sulfate [SDS], and 100 μl of denatured salmon sperm DNA. Membranes were prehybridized for at least 2 h at 65°C. The probe used in these experiments was a double-stranded NdeI-BstXI fragment of the CP cDNA, which encompasses the majority of the CP coding region and therefore hybridizes to plus and minus strands of genomic RNA3 and to the positive-stranded subgenomic RNA4. The DNA fragment was labeled with [α-^{32}P]dCTP (PerkinElmer) by using the Prime-It II kit (Stratagene). Unincorporated nucleotide was removed using a Chromaspin gel filtration column (ClonTech). After heat-denaturing the probe, it was added directly to the prehybridization solution and hybridization proceeded overnight at 65°C. The membrane was washed twice for 10 min at room temperature in 2× SSC (0.3 M NaCl, 0.03 M sodium citrate, pH 7)–0.1% SDS and once for 10 min at room temperature in 0.2× SSC (0.03 M NaCl, 0.003 M sodium citrate, pH 7)–0.1% SDS. Membranes were wrapped in plastic wrap and exposed to X-ray film.

AMV protein analysis. Two milliliters of protoplast suspension was sedimented and resuspended in 150 μl of NT-1 extraction buffer (0.1 M $KHPO_4$, 1 mM EDTA, 10 mM dithiothreitol, 5% glycerol). The cells were lysed by sonication and centrifuged for 15 min at 12,000 × *g* at 4°C. Next, 20 μl of supernatant in 1× SDS was analyzed by electrophoresis into a 12% polyacrylamide–SDS gel. AMV CP was detected by Western blotting with a polyclonal anti-AMV CP antibody and chemifluorescence detection (Amersham Biosciences).

RESULTS

AMV-peptide interactions compact the RNA conformation. In the conformational switch model, Olsthoorn et al. (22) proposed that CP binding converts the 3′-terminal conformation of the AMV RNAs from a compact TLS to an extended linear form that inhibits minus-strand synthesis. Prior published evidence suggested that CP peptide binding to the RNA 3′ terminus has the opposite effect; that is, it compacts the RNA conformation (3). To further evaluate the effects of CP binding on the AMV RNA 3′ conformation, EMSA and gel filtration chromatography analyses were applied. For these assays, a 26-amino-acid N-terminal peptide (CP26) representing the CP RNA binding domain (Fig. 1A) was incubated with the 170-nucleotide 3′ UTR common to viral RNA3 and -4 (Fig. 1B). Peptide CP26 binding has been shown to yield RNA protection patterns indistinguishable from those of full-length viral CP by hydroxyl radical footprinting experiments (2). Consistent with our published findings (3), adding increasing amounts of CP26 to the 170-nucleotide RNA yielded a series of complexes (Fig. 2A, lanes 2 through 5) that migrate faster than unbound RNA (Fig. 2, lane 1) through nondenaturing gels. The specificity of the peptide binding was confirmed in binding experiments that used the point mutant peptide CP26R17A, which has significantly diminished RNA binding potential (2) and does not elicit RNA band shifts (Fig. 2B, lanes 1 through 5). We interpreted the increased mobility of the RNA-CP26 complexes as evidence that the RNA collapses through a series of increasingly compact conformers.

To provide an additional analysis of the RNA conformational changes, the hydrodynamic profile of the RNA-CP26 complex was evaluated by analytical size exclusion chromatography. In the absence of CP26, the RNA elutes from the size exclusion column at 21.22 min (Fig. 2C). In the presence of excess CP26, the RNA-CP26 complex has a retention time of 21.84 min, indicating a smaller Stokes radius. Taken together, the EMSA and gel filtration data strongly suggest that the

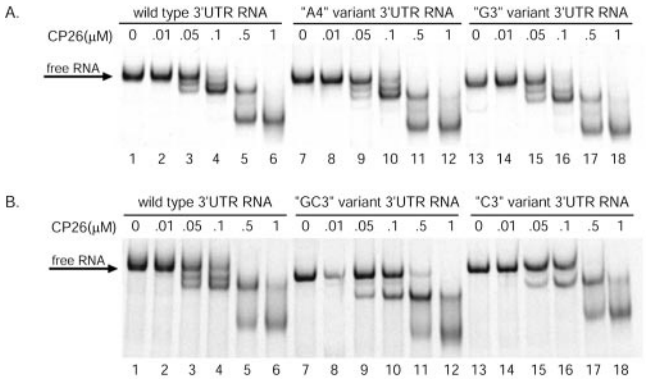

FIG. 3. Peptide CP26 binds to wild-type and pseudoknot mutant RNAs. The A4, G3, C3, and GC3 nucleotide substitutions were described by Olsthoorn et al. (22). RNA-peptide binding reactions were analyzed by electrophoresis into a nondenaturing polyacrylamide gel as described in Materials and Methods. The RNA concentration in the binding reactions was 20 nM. Peptide concentrations used in the binding reactions are indicated above each lane. (A) Mobility shift analysis of wild-type 170-nucleotide AMV RNA (lanes 1 through 6), the A4 variant RNA (lanes 7 through 12), and the G3 variant RNA (lanes 13 through 18). (B) Mobility shift analysis of wild-type 170-nucleotide AMV RNA (lanes 1 through 6), GC3 variant RNA (lanes 7 through 12), and C3 RNA (lanes 13 through 18).

interaction of the viral CP with the RNA compacts the RNA structure rather than extends it, as suggested by the conformational switch model.

Peptide and CP binding to proposed pseudoknot variant RNAs. The conformational switch model proposes that the 3′ termini of the AMV RNAs exist in two mutually exclusive conformations: the CP-free pseudoknotted structure and the CP-bound extended conformation (22). Since an experimental analysis of CP or CP peptide binding to several of the pseudoknot variant RNAs (Fig. 1C) has not been described previously, experiments were performed using variant RNAs containing mutations in the proposed pseudoknot pairing nucleotides (22). To evaluate the role of the proposed pseudoknot in CP binding, we used three variant RNAs, referred to as A4, G3, and C3, containing nucleotide substitutions that disrupt the proposed pseudoknot, in addition to one variant RNA, referred to as GC3, containing compensatory nucleotide substitutions that reestablish the potential for pseudoknot pairings. The details of the pseudoknot mutations, obtained using RNA4 numbering terminology, are as follows (Fig. 1B and C): A4 changes nucleotides 789 through 792 (region 1) to AAAA, G3 changes nucleotides 790 through 792 (region 1) to GGG, and C3 converts nucleotides 869 through 871 (region 3) to GGG and nucleotides 875 through 877 (region 2) to CCC. The variant RNA GC3 combines the nucleotide changes of G3 and C3 to restore the potential pseudoknot base pairing.

The EMSA results (Fig. 3) are evidence that the CP26 peptide binds with similar affinities to the wild-type RNA (Fig. 3, lanes 1 through 6), proposed pseudoknot-disrupted RNAs (Fig. 3A, lanes 7 through 18, and B, lanes 13 through 18), and the GC3 pseudoknot mutant RNA containing compensatory pairing interactions (Fig. 3B, lanes 7 through 12). Reusken et al. (25) reported previously that a variant RNA containing the GC3 mutation (referred to therein as 3KSL1-8) retained CP binding potential. Competitive binding assays were done to further evaluate the CP binding potentials of the pseudoknot variant RNAs. Here, unlabeled wild-type or pseudoknot variant RNAs were mixed with radiolabeled wild-type RNA prior to adding CP peptide. Titration of the respective unlabeled RNAs yielded similar patterns of competitive binding, as analyzed by native gel electrophoresis (data not shown), demonstrating that the introduction of the pseudoknot nucleotide substitutions (Fig. 1C) did not have a dramatic effect upon CP binding in vitro.

We anticipated that the GC3 RNA, containing nucleotide substitutions that restore the proposed pseudoknot pairing potential, would have electrophoretic properties similar to those of the wild-type RNA. Interestingly, the protein-free GC3 variant RNA (Fig. 3B, lane 7) migrated with faster mobility than the wild-type RNA (Fig. 3B, lane 1). These data suggested that the conformations of the wild-type and GC3 covarying RNAs are not equivalent.

To extend the analysis, we tested the virion CP binding to the 170-nucleotide wild type and to the A4 and G3 pseudoknot-disrupted RNAs. The A4 and G3 constructs were chosen for this analysis because they maintain wild-type base pairing potential in the 3′ hairpin. The binding reactions were carried out using our reported conditions (1, 2, 14). The multiple shifted bands (Fig. 4A, lanes 1 through 5) were consistent with prior evidence showing that multiple CP dimers interact with the 3′ UTR of the wild-type AMV RNAs (14, 24). The results also demonstrated that CP binds to the variant A4 and G3 RNAs (Fig. 4A, lanes 6 through 15). The CP binding results were consistent with the binding data observed using the CP26 peptide (Fig. 3).

Elevated magnesium concentrations do not severely inhibit peptide or CP binding. As support for the conformational switch model, Olsthoorn et al. (22) reported that elevated magnesium concentrations severely inhibited CP binding to the wild-type RNA but not to a pseudoknot variant RNA. The interpretation of these results was that magnesium stabilized the pseudoknot conformation (9), which blocked CP binding. The reported magnesium binding reactions were done under conditions of RNA excess over the CP where a small percentage of the probe RNA was bound to protein (22). To explore the effects of magnesium on CP binding, we titrated CP at concentrations in excess over the input-labeled RNA while testing different magnesium concentrations in the renaturation and binding reactions. Both the 170-nucleotide wild-type and pseudoknot-deficient A4 and G3 RNA fragments were tested. In contrast to the conformational switch model, the data shown in Fig. 4B provide evidence that renaturing the AMV RNA in 15 mM magnesium, followed by incubation with CP in a buffer containing 10 mM magnesium, does not severely inhibit CP binding to wild-type RNA (Fig. 4B, lanes 1 through 5). Although we did not find that high magnesium levels blocked CP binding, the data suggested that high magnesium levels have small effects on binding affinity (i.e., a less than twofold effect on the K_d [6], compare lanes 3 of Fig. 4A and B).

To distinguish between a nonspecific magnesium effect and a specific effect due to stabilizing the proposed pseudoknot, we examined CP binding to the A3 and G4 RNAs at elevated magnesium concentrations. The prediction from the confor-

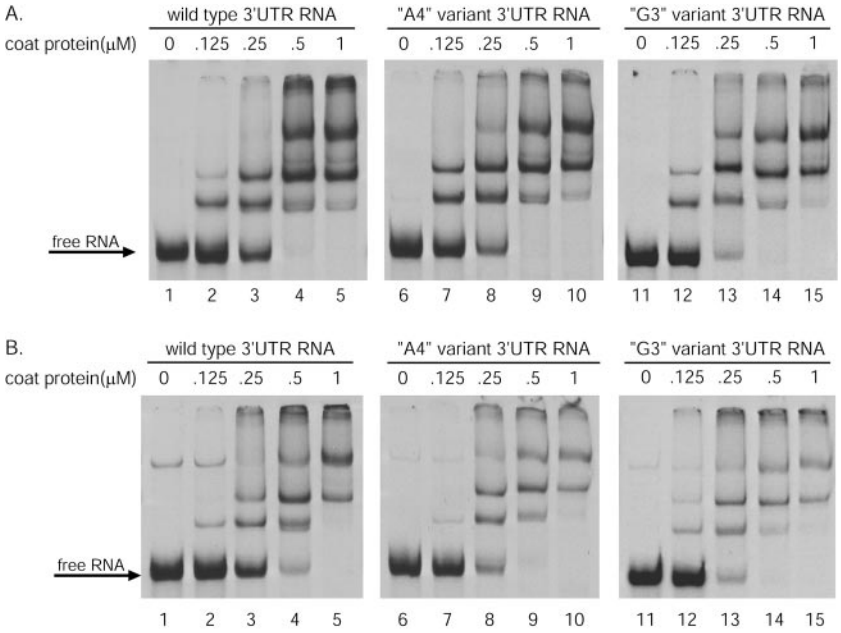

FIG. 4. The AMV CP binds to wild-type and pseudoknot mutant RNAs in the absence or presence of elevated magnesium concentrations. The A4 and G3 nucleotide substitutions were described by Olsthoorn et al. (22). RNA-CP binding reactions were analyzed by electrophoresis into a nondenaturing polyacrylamide gel as described in Materials and Methods. CP concentrations used in the binding reactions are indicated above each lane. (A) Mobility shift analysis of RNA-CP complexes under standard conditions: with renaturation buffer (3 mM magnesium) or binding buffer (0 mM magnesium). Wild-type 170-nucleotide AMV RNA (lanes 1 through 5), A4 variant RNA (lanes 6 through 10), and G3 variant RNA (lanes 11 through 15) are shown. (B) Native polyacrylamide gel electrophoretic separation of wild-type and pseudoknot variant RNAs in complex with viral CP. The RNA renaturation buffer contained 15 mM magnesium, and the protein binding buffer contained 10 mM magnesium. Wild-type 170-nucleotide AMV RNA (lanes 1 through 5), A4 variant RNA (lanes 6 through 10), and G3 variant RNA (lanes 11 through 15) are shown.

mational switch model is that these RNAs should be not be affected by magnesium because of their inability to form the region 1-region 2 pseudoknot. However, the data demonstrate that magnesium has slight effects on CP binding affinities for the pseudoknot variant RNAs in a manner similar to that observed with the wild-type RNA (compare lanes 2, 7, and 12 of Fig. 4A and B). The results presented in Fig. 4 are evidence that elevated magnesium levels do not severely inhibit CP binding to the viral RNAs. The slight decrease in CP affinities observed at high magnesium levels is likely due to a direct effect of the magnesium ions, perhaps by shielding charges on the RNA or CP, rather than to stabilization of the pseudoknot structure.

To provide a more detailed analysis of the effects of magnesium concentration on CP binding, we tested CP26 peptide binding to the wild-type 3′ UTR in the presence of increasing magnesium concentrations. By applying the conditions used to develop the RNA conformational switch model (22), the 170-nucleotide RNA fragment (Fig. 1B) was renatured in buffered solutions containing 3 to 15 mM magnesium, followed by incubation with peptide CP26 in binding buffer containing 0 to 10 mM magnesium. Again, we observed that, in contrast to the RNA conformational switch model, CP26 peptide binding is not severely inhibited when extra magnesium is added to the renaturation and/or binding reactions. The shift patterns (Fig. 5) were qualitatively similar over a wide range of magnesium concentrations used in the RNA renaturation and peptide binding solutions. As described for CP binding above (Fig. 4),

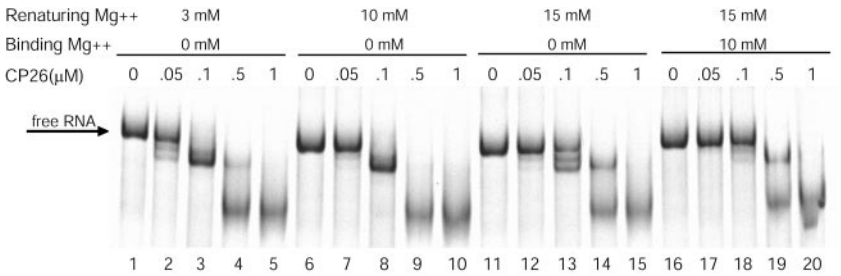

FIG. 5. Increased magnesium concentrations do not block peptide binding to the wild-type RNA. The figure shows a native polyacrylamide gel electrophoretic separation of wild-type RNAs in the presence of increasing concentrations of AMV peptide CP26 and varying magnesium levels present in the RNA renaturation and peptide binding buffers (see Materials and Methods for details). The peptide concentrations and magnesium concentrations used in the RNA renaturation and RNA-peptide binding reactions are shown above the respective gel lanes.

elevated magnesium levels correlated with slight decreases in peptide binding affinities (Fig. 5, compare lanes 3, 8, 13, and 18); however, the results shown in Fig. 4 suggest that high magnesium levels have an inherent effect on CP binding unrelated to pseudoknot stabilization. Comparing conditions with those of Olsthoorn et al. (22), one difference to note is that our binding experiments, with both the CP26 peptide and CP, are done using RNA concentrations that are lower than the K_d of the wild-type binding interaction (1) and with protein in excess (7). We conclude from these data that, in contrast to the conformational switch model, elevated magnesium levels do not severely inhibit CP or peptide binding to the wild-type 3′ UTR RNA. The biochemical data presented here provide evidence that the viral CP binding to the AMV RNA 3′ UTR is independent of the proposed pseudoknot shown in Fig. 1B (22).

RNA3 containing the pseudoknot compensatory mutant GC3 does not replicate in nontransgenic cells. A principal experimental justification for the conformational switch model was the observation that replication activity was disrupted by mutating the pseudoknot pairing nucleotides but rescued when compensatory mutations that restore pseudoknot pairing were introduced into the RNA. We repeated the functional assays using infectious variant genomic RNA3 clones that contained the A4, G3, C3, and GC3 substitutions at the 3′ terminus. However, unlike the approach described by Olsthoorn et al. (22), nontransgenic tobacco protoplasts were used for the replication assay. The variant RNA3 molecules were cotransfected with genomic RNA1 and -2 (providing the helicase-methyltransferase and replicase activities, respectively) and RNA4 (to provide CP needed to activate replication). A truncated activator, RNA4 (AMV4-trUTR), wherein nucleotides 719 through 842 of the 3′ untranslated region (Fig. 1B) were deleted (26) was used for these experiments. AMV4-trUTR permitted us to distinguish input RNA4 (AMV4-trUTR) from subgenomic RNA4 transcribed from minus-strand RNA3 during replication. Replication was assayed by Western blotting to detect CP production (Fig. 6A) and by Northern blotting to detect subgenomic RNA4 expression (Fig. 6B).

Control experiments for the replication assays are presented in Fig. 6, lanes 1 through 3. Although the transfected activator RNA4 (AMV4-trUTR) alone could be detected by Northern blotting (Fig. 6B, lane 1), its translation product, CP, was not detected by immunoblotting in the absence of viral RNA replication (Fig. 6A, lane 1). RNA1, -2, and -3 alone were not infectious, and neither CP nor subgenomic RNA was observed (Fig. 6, lanes 2). In comparison, both CP and subgenomic RNA4 were detectable when wild-type RNA1, -2, and-3 plus AMV4-trUTR were transfected into the cells (Fig. 6, lanes 3). The results of testing the pseudoknot mutants are shown in lanes 4 through 7. In agreement with published results (22), we found that the A4, G3, and C3 mutations all interfered with replication, as evidenced by the absence of viral CP and subgenomic RNAs. However, contrary to data reported previously (22), the compensatory GC3 substitutions did not rescue functional activity in replication (Fig. 6, lanes 6). The entire infectious RNA3 clone carrying the GC3 covarying nucleotides was sequenced to confirm that no mutations other than the GC3 substitutions were present. These data, which are representative of three independent trials, demonstrate that the nucleotide changes proposed to both disrupt and restore the pseudoknot structure are deleterious to replication. These results do not support the significance of the proposed pseudoknot structure for regulating replication.

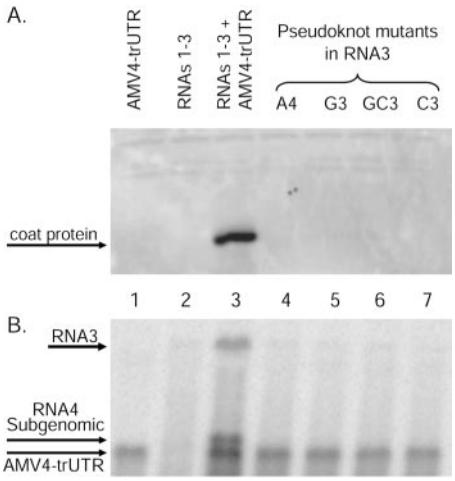

FIG. 6. Compensatory nucleotide changes in the pseudoknot variant RNAs do not rescue functional activity in viral RNA replication. The A4, G3, C3, and GC3 nucleotide changes were introduced into infectious clones of viral RNA3. Variant RNA3 and wild-type RNA1 and -2 were transfected into NT-1 tobacco cells by electroporation along with the 3′-UTR-truncated activator RNA4 (AMV4-trUTR) (see Materials and Methods). Viral RNA replication was assayed by examining viral CP expression (A) and by the appearance of subgenomic viral RNA (B). Cells were transfected with the following RNAs or mixtures of RNAs: lane 1, truncated activator CP mRNA (AMV4-trUTR) only; lane 2, wild-type viral RNA1, -2, and -3; lane 3, wild-type viral RNA1, -2, and -3 plus AMV4-trUTR; lanes 4 through 7: wild-type RNA1 and -2 and AMV4-trUTR along with variant RNA3 constructs containing the A4, G3, GC3, and C3 mutations, respectively. The detection of viral CP and subgenomic RNA (lanes 3) is evidence of viral RNA replication.

Effects of the pseudoknot mutations in RNA4 on the activation of replication. One possible interpretation of the effects of the pseudoknot mutations on RNA replication (22) (Fig. 6) is that the mutations inserted into RNA3 and copied into the subgenomic RNA4 (CP mRNA) may limit viral mRNA translation and consequently decrease viral replication. This suggestion is based on reports that CP binding may regulate AMV RNA translation (20, 21). To distinguish between effects the pseudoknot mutations may have on replication and translation, the nucleotide changes were introduced into the full-length 3′ UTR of RNA4. We assayed the ability of these variant RNAs to activate replication by transfecting wild-type RNA1, -2, and -3 along with variant RNA4, as described previously (16, 26). We have shown previously that, using this approach, virus replication levels correlate with CP translation efficiency (26). If the mechanism underlying the absence of replication observed using variant RNA3 constructs (Fig. 6) were due to diminished RNA4 translation, the expected result would be that activator RNA4 containing the same 3′ UTR mutations would fail to activate replication.

Western blot analysis revealed that RNA4 constructs corresponding to all four pseudoknot mutants were functional in activating viral RNA replication, as evidenced by the detection of viral CP (Fig. 7, lanes 3 through 6). The levels of activation

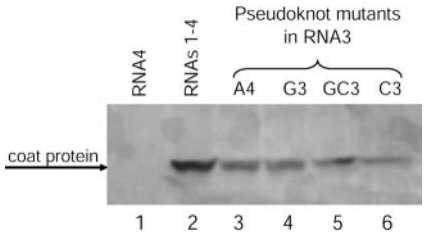

FIG. 7. Variant RNA4 constructs containing the A4, G3, C3, and GC3 mutations activate viral RNA replication. The A4, G3, C3, and GC3 nucleotide changes were cloned into full-length RNA4. These variant RNA4 constructs were then cotransfected with wild-type viral RNA1, -2, and -3. Viral RNA replication was assayed by Western blotting for the viral CP. Lane 1, wild-type viral RNA1, -2, and -3; lane 2, wild-type viral RNA1 through RNA4; lanes 3 through 6, all cells transfected with wild-type RNA1, -2, and -3 along with variant RNA4 constructs containing the A4, G3, GC3, and C3 mutations, respectively. The detection of viral CP is evidence of the activation of viral RNA replication.

observed for the four variant RNA4 constructs were clearly detectable but lower than wild-type levels (Fig. 7, compare lanes 3 through 6 with lane 2). We considered the possibility that the decreased amounts of CP translated from the variant RNA4 constructs (Fig. 7) were insufficient to promote ongoing replication. However, previous data (26) demonstrated that a G851A:G860U mutation that caused a similar decrease in RNA4 translation did not diminish viral RNA replication significantly when introduced into RNA3. These results suggest that the defects associated with the pseudoknot mutations in genomic RNA3 (Fig. 6) correlate principally with viral RNA replication rather than translation.

Based on the conformational switch model (22), we anticipated that inserting covarying nucleotides to restore pseudoknot pairing in the GC3 mutant would generate an RNA that had wild-type functional activity in both replication and translation. The data (Fig. 3, 6, and 7) provide evidence suggesting that compensatory GC3 variant RNA3 and -4 indeed are not functionally equivalent to the wild-type RNA. These results do not support the conclusion that a pseudoknot represents a molecular switch that regulates minus-strand AMV RNA synthesis.

DISCUSSION

In this report, we describe experiments aimed at understanding why AMV CP is required to activate viral RNA replication. In previous work, Olsthoorn et al. (22) proposed the conformational switch model to explain the activation of AMV replication and the switch from minus- to plus-strand RNA synthesis. This model argues that CP binding extends the viral RNA conformation, in contrast to previously published data from our laboratory indicating that the RNA conformation is compacted upon CP peptide binding (3). Olsthoorn et al. also reported that elevated magnesium concentrations block CP binding, a result that we had not observed. In an attempt to resolve or understand the differences in data and interpretations, we repeated key experiments reported to support the conformational switch model (22). Our conclusion is that the data reported here support an alternate model, the 3′ organization model.

The defining concept of the 3′ organization model is that the replication strategies of the bromoviruses are united not by the presence of a TLS but rather by the requirement for a structurally organized 3′ terminus. Placing AMV and ilarviruses in the mold of a TLS is an imperfect fit that is inconsistent with the definitions of tRNA-like sequences. AMV and ilarvirus RNAs do not display prototypical features that define a TLS. They lack the canonical 3′ CCA terminus and they cannot be aminoacylated (13), nor do they serve as efficient substrates for the CCA repair enzyme nucleotidyltransferase (22). Furthermore, if we do assume that all of the bromovirus RNAs share the pseudoknotted tRNA-like 3′ terminus, it is difficult to rationalize why AMV and ilarviruses alone would require CP to disrupt the proposed common pseudoknot in order to permit plus-strand synthesis. We argue that the distinctive AUGC tetranucleotide repeats in the 3′ RNA sequence, the unique requirement for CP to activate replication, and the absence of a canonical TLS suggest that AMV and ilarviruses have adopted a different replication mechanism while sharing a unifying feature with other bromovirus RNAs: the importance of a structurally organized end. This structural organization is provided by a TLS for many bromoviruses but uniquely by an RNA-CP complex in the examples of AMV and ilarviruses.

Evidence for 3′ organization is provided by the crystal structure of the 3′-terminal 39 nucleotides of the AMV RNA in complex with the RNA binding domain of the viral CP (11). These data show that the RNA binding domain of the viral CP forms an α-helix containing a crucial arginine (Fig. 1A) (2) that stabilizes the formation of additional base pairs between the AUGC repeats that characterize the 3′ UTR sequences of these RNAs. By forming these additional base pairs, the RNA becomes conformationally constrained and also compacted, as suggested by biochemical data (Fig. 2) (3). The compacted, organized AMV RNA-CP complex is proposed here as the functional equivalent of a TLS. The outcome of these conformational changes would be to present a uniform population of termini to act as templates for viral RNA replication. The 3′ organization model argues that CP binding to the viral RNAs is required for replication because it establishes the conformational features needed for recognition and accurate initiation of viral RNA replication.

Some of the results presented here contrast with those reported by others. One line of evidence reported in support of the pseudoknot and its effects on CP binding was the inhibitory effects of elevated magnesium concentration upon CP binding in vitro (22). We analyzed CP binding to both wild-type and pseudoknot variant RNAs over a range of protein concentrations, using the same magnesium concentrations reported previously (22). The data (Fig. 4 and 5) demonstrate that elevated magnesium levels do not severely inhibit CP binding, as reported previously (22). We note that the interpretation of the data in Fig. 4 and 5 is facilitated by the presentation of a titration series of CP concentrations and by using CP in excess over the RNA. By this approach, the effects of the magnesium can be assessed with greater resolution because binding over a range of both magnesium and peptide or coat protein concentrations is presented using conditions wherein all of the RNA can be shifted into complexes. This contrasts with the data

presented by Olsthoorn et al. wherein only a small percentage of the RNA was capable of binding CP (i.e., the RNA was in large excess) and only a single concentration of increased magnesium was presented.

By substituting the nucleotides in the proposed pseudoknot pairing region, Olsthoorn et al. (22) showed that viral RNA replication was disrupted. We agree with the results of Olsthoorn et al. indicating that the A4, G3, and C3 mutations disrupt viral RNA replication (Fig. 6); however, disruption of replication by the A4, G3, and C3 mutations does not, by definition, prove the pseudoknot. The compelling evidence for the significance of the pseudoknot was suggested by the functional rescue provided by the introduction of covarying nucleotide changes that altered the nucleotide sequence but reestablished pseudoknot base pairing (22). However, we demonstrate here that when nontransgenic tobacco protoplasts are used for the viral RNA replication assay, the compensatory substitutions predicted to restore pseudoknot pairing (GC3) do not rescue functional activity (Fig. 6, lane 6), nor does the covarying RNA migrate with the wild-type RNA (Fig. 3B, lane 7). Although these data raise questions about the functional role of the pseudoknot in replication, they do suggest that the mutated nucleotides are somehow important for replication. The A4, G3, C3, and GC3 mutations can be added to a collection of 3′ nucleotide substitutions that disrupt replication. In general, AMV RNA replication is sensitive to nucleotide substitutions in the 3′ UTR, and a number of changes outside of the pseudoknot have also been shown to affect viral RNA replication in this system (16, 26). The molecular basis for the effects on replication is largely unknown, but others have shown that viral RNA replication can be affected by both *cis* and *trans* mutations in positive-strand RNA viruses (17).

The functional experiments reported by Olsthoorn et al. (22) in support of the pseudoknot were carried out using transgenic plants and protoplasts that constitutively express the viral P1 and P2 replicase proteins. The transgenic P1 and P2 plants and protoplasts, in contrast to native tissue and contrary to a defining characteristic of AMV and ilarviruses, replicate the viral RNAs in the absence of the viral CP (29). We propose that the use of transgenic plants that constitutively express replicase proteins may introduce experimental artifacts that complicate the analysis of viral RNA replication mechanisms. Recent evidence suggests that significant intracellular membrane rearrangements are caused by the expression of bromovirus replicase proteins (27), potentially affecting viral RNA replication by creating an environment that differs substantially from that present in a very early native infection. Smirnyagina et al. (28) reported that N-terminal sequences of the brome mosaic virus 2a polymerase protein were dispensable for brome mosaic virus RNA replication when expressed from DNA plasmids, but different results were found under native infection conditions. In native infections, the 120 N-terminal amino acids of the 2a replicase protein were found to be necessary and sufficient for localization to the endoplasmic reticulum membrane as mediated by interactions with the 1a protein (28). These data suggest that transgenic cells and tissues that constitutively express P1 and P2 do not reflect the intracellular environment of an early viral infection. For this reason, nontransgenic cells were used in our experiments to examine the requirements for early replication. The differences in experimental approaches may explain the contrasting results from the two laboratories.

Although we did not find evidence for pseudoknot-mediated regulation of the early phases of viral RNA replication, we performed an additional experiment that was designed to directly test for pseudoknot formation. Comolli et al. (8) explored the potential for pseudoknot formation in the telomerase ribonucleoprotein complex by assaying for transpseudoknot formation between two RNA fragments. We mixed the labeled 180-mer 3′ UTR RNA (Fig. 1B) with increasing concentrations (0- to 100-fold molar excess) of the 39-nucleotide 3′-terminal RNA fragment and then denatured at 90°C and reannealed the RNAs by slow cooling in a buffered salt solution. Native polyacrylamide gel electrophoresis was used to test for the formation of RNA heterodimers representing pairing at the proposed pseudoknot region (i.e., between region 2 of the 39-mer RNA and region 1 of the 180-mer fragment [Fig. 1B]). Although conditions similar to these showed transpseudoknot pairing with the telomerase RNA fragments, as reflected by complexes with diminished electrophoretic mobility on native polyacrylamide gels (8), no intermolecular pairing was observed with the AMV RNA fragments (data not shown). The interpretation of these results is limited to stating that we looked for pseudoknot formation in the AMV RNA by using conditions known to detect these interactions (8), but none was observed. The potential significance of the covarying nucleotide sequences found in a comparative analysis of region 1 and 2 sequences among AMV and the ilarviruses (Fig. 1C) (22) remains open. It is both interesting and puzzling that the nucleotide sequences in regions 1 and 3 seem to covary simultaneously with those in region 2 to maintain the potential to form competing short- and longer-range secondary structures.

In conclusion, we were unable to reproduce key experiments that have been reported to substantiate the conformational switch model. Consequently, we find insufficient evidence to confirm that model, wherein two different AMV RNA conformations, a pseudoknotted versus an extended RNA form, represent a molecular switch that controls the transcription of minus and plus AMV RNA strands. Therefore, we propose the 3′ organization model as a framework to understand the structural features of the AMV and ilarvirus RNAs and the role of the viral CP in activating viral RNA replication. The 3′ organization model does not explain the switch from translation to replication; however, we speculate that CP occupancy on the multiple CP binding sites (14, 24), as determined by CP concentration, may have a regulatory role.

ACKNOWLEDGMENT

This work was supported by Public Health Service grant GM42504 from the National Institutes of Health.

REFERENCES

1. **Ansel-McKinney, P., and L. Gehrke.** 1998. RNA determinants of a specific RNA-coat protein peptide interaction in alfalfa mosaic virus: conservation of homologous features in ilarvirus RNAs. J. Mol. Biol. **278:**767–785.
2. **Ansel-McKinney, P., S. W. Scott, M. Swanson, X. Ge, and L. Gehrke.** 1996. A plant viral coat protein RNA binding consensus sequence contains a crucial arginine. EMBO J. **15:**5077–5084.
3. **Baer, M., F. Houser, L. S. Loesch-Fries, and L. Gehrke.** 1994. Specific RNA binding by amino-terminal peptides of alfalfa mosaic virus coat protein. EMBO J. **13:**727–735.
4. **Buchmueller, K. L., A. E. Webb, D. A. Richardson, and K. M. Weeks.** 2000. A collapsed non-native RNA folding state. Nat. Struct. Biol. **7:**362–366.

5. **Calnan, B. J., S. Biancalana, D. Hudson, and A. D. Frankel.** 1991. Analysis of arginine-rich peptides from the HIV Tat protein reveals unusual features of RNA protein recognition. Genes Dev. **5:**201–210.
6. **Calnan, B. J., B. Tidor, S. Biancalana, D. Hudson, and A. D. Frankel.** 1991. Arginine-mediated RNA recognition: the arginine fork. Science **252:**1167–1171.
7. **Carey, J., and O. C. Uhlenbeck.** 1983. Kinetic and thermodynamic characterization of the R17 coat protein-ribonucleic acid interaction. Biochemistry **22:**2610–2615.
8. **Comolli, L. R., I. Smirnov, L. Xu, E. H. Blackburn, and T. L. James.** 2002. A molecular switch underlies a human telomerase disease. Proc. Natl. Acad. Sci. USA **99:**16998–17003.
9. **Draper, D. E.** 1996. Strategies for RNA folding. Trends Biochem. Sci. **21:**145–149.
10. **Friederich, M. W., F. U. Gast, E. Vacano, and P. J. Hagerman.** 1995. Determination of the angle between the anticodon and aminoacyl acceptor stems of yeast phenylalanyl tRNA in solution. Proc. Natl. Acad. Sci. USA **92:**4803–4807.
11. **Guogas, L., D. Filman, J. Hogle, and L. Gehrke.** 2004. Cofolding organizes alfalfa mosaic virus RNA and coat protein for replication. Science **306:**2108–2111.
12. **Guogas, L. M., S. M. Laforest, and L. Gehrke.** 2005. Coat protein activation of alfalfa mosaic virus replication is concentration dependent. J. Virol. **79:**5752–5761.
13. **Hall, T. C.** 1979. Transfer RNA-like structures in viral genomes, p. 1–26. *In* G. H. Bourne and J. R. Danielli (ed.), International review of cytology, vol. 60. Academic Press, New York, N.Y.
14. **Houser-Scott, F., M. L. Baer, K. F. Liem, Jr., J.-M. Cai, and L. Gehrke.** 1994. Nucleotide sequence and structural determinants of specific binding of coat protein or coat protein peptides to the 3′ untranslated region of alfalfa mosaic virus RNA 4. J. Virol. **68:**2194–2205.
15. **Kruseman, J., B. Kraal, E. Jaspars, J. Bol, F. Brederode, and H. Veldstra.** 1971. Molecular weight of the coat protein of alfalfa mosaic virus. Biochemistry **10:**447–455.
16. **Laforest, S. M., and L. Gehrke.** 2004. Spatial determinants of the alfalfa mosaic virus coat protein binding site. RNA **10:**48–58.
17. **Lindenbach, B. D., J.-Y. Sgro, and P. Ahlquist.** 2002. Long-distance base pairing in flock house virus RNA1 regulates subgenomic RNA3 synthesis and RNA2 replication. J. Virol. **76:**3905–3919.
18. **Loesch-Fries, L. S., N. P. Jarvis, K. J. Krahn, S. E. Nelson, and T. C. Hall.** 1985. Expression of alfalfa mosaic virus RNA 4 cDNA transcripts *in vitro* and *in vivo.* Virology **146:**177–187.
19. **Murphy, F. L., Y. H. Wang, J. D. Griffith, and T. R. Cech.** 1994. Coaxially stacked RNA helices in the catalytic center of the Tetrahymena ribozyme. Science **265:**1709–1712.
20. **Neeleman, L., H. J. Linthorst, and J. F. Bol.** 2004. Efficient translation of alfamovirus RNAs requires the binding of coat protein dimers to the 3′ termini of the viral RNAs. J. Gen. Virol. **85:**231–240.
21. **Neeleman, L., R. C. Olsthoorn, H. J. Linthorst, and J. F. Bol.** 2001. Translation of a nonpolyadenylated viral RNA is enhanced by binding of viral coat protein or polyadenylation of the RNA. Proc. Natl. Acad. Sci. USA **98:**14286–14291.
22. **Olsthoorn, R. C., S. Mertens, F. T. Brederode, and J. F. Bol.** 1999. A conformational switch at the 3′ end of a plant virus RNA regulates viral replication. EMBO J. **18:**4856–4864.
23. **Quigley, G. J., L. Gehrke, D. A. Roth, and P. E. Auron.** 1984. Computer-aided nucleic acid secondary structure modeling incorporating enzymatic digestion data. Nucleic Acids Res. **12:**347–366.
24. **Reusken, C. B. E. M., L. Neeleman, and J. F. Bol.** 1994. The 3′-untranslated region of alfalfa mosaic virus RNA 3 contains at least two independent binding sites for viral coat protein. Nucleic Acids Res. **22:**1346–1353.
25. **Reusken, C. B., L. Neeleman, F. T. Brederode, and J. F. Bol.** 1997. Mutations in coat protein binding sites of alfalfa mosaic virus RNA 3 affect subgenomic RNA 4 accumulation and encapsidation of viral RNAs. J. Virol. **71:**8385–8391.
26. **Rocheleau, G., J. Petrillo, L. Guogas, and L. Gehrke.** 2004. Degenerate in vitro genetic selection reveals mutations that diminish alfalfa mosaic virus RNA replication without affecting coat protein binding. J. Virol. **78:**8036–8046.
27. **Schwartz, M., J. Chen, W. M. Lee, M. Janda, and P. Ahlquist.** 2004. Alternate, virus-induced membrane rearrangements support positive-strand RNA virus genome replication. Proc. Natl. Acad. Sci. USA **101:**11263–11268.
28. **Smirnyagina, E., N. S. Lin, and P. Ahlquist.** 1996. The polymerase-like core of brome mosaic virus 2a protein, lacking a region interacting with viral 1a protein in vitro, maintains activity and 1a selectivity in RNA replication. J. Virol. **70:**4729–4736.
29. **Taschner, P. E. M., A. C. Vanderkuyl, L. Neeleman, and J. F. Bol.** 1991. Replication of an incomplete alfalfa mosaic virus genome in plants transformed with viral replicase genes. Virology **181:**445–450.
30. **Walter, F., A. I. Murchie, D. R. Duckett, and D. M. Lilley.** 1998. Global structure of four-way RNA junctions studied using fluorescence resonance energy transfer. RNA **4:**719–728.
31. **Watanabe, Y., T. Meshi, and Y. Okada.** 1987. Infection of tobacco protoplasts with in vitro transcribed tobacco mosaic virus RNA using an improved electroporation method. FEBS Lett. **219:**65–69.
32. **Webb, A. E., and K. M. Weeks.** 2001. A collapsed state functions to self-chaperone RNA folding into a native ribonucleoprotein complex. Nat. Struct. Biol. **8:**135–140.